Potential Energy Surfaces for Tc + CO, Re + CO, and Ta + CO and Periodic Trends of the Second- and Third-Row Transition Metals Interaction with CO

Hang Tan and Muzhen Liao

Center for Advanced Study and Department of Chemistry, Tsinghua University, Beijing 100084, China

Dingguo Dai and K. Balasubramanian*

Department of Chemistry and Biochemistry, Arizona State University, Tempe, Arizona 85287-1604

Received: November 16, 1998; In Final Form: February 3, 1999

While other third-row transition metals react more readily with CO, rhenium carbon monoxide is found to be relatively less stable at both the complete active space multiconfiguration self-consistent field (CASMCSCF) and the multireference singles + doubles configuration interaction (MRSDCI) computation levels. The $^4\Sigma^-$ state was found to be the ground state for both TcCO and ReCO complexes. Although at the CASSCF level this state has negative D_e relative to the M(a^6S) + CO($^1\Sigma^+$) dissociation limit (M = Tc or Re), at a more accurate MRSDCI level, the D_e's of the $^4\Sigma^-$ state were computed as 0.002 eV for TcCO, and 0.012 eV for ReCO, with respect to the same dissociation limit. Spin−orbit effects for ReCO and TaCO split the $^4\Sigma^-$ nonrelativistic ground state into $^1/_2$ and $^3/_2$ Ω states. The energy difference for the two states is computed as 981 cm^{-1}. For the TaCO complex, the spin−orbit effects enlarge the energy difference between $^4\Delta_{1/2}$ and $^6\Sigma^+_{1/2}$ to 1742 cm^{-1}, compared with 691 cm^{-1} in the absence of spin−orbit effects. The computed properties of all M−CO species (M = second- and third-row transition metals) and their nature of bonding for TcCO and ReCO are discussed. It is shown that the curve crossing of the ground and excited states is an important factor in the nature of charge transfer in these species. This combined with the extent of charge transfer from CO to M, and the back transfer from M to CO through π-bonding, is found to be important to result in stable complexes.

I. Introduction

Reactivity of transition metal with CO, and especially of the IVB through VIIIB groups, has been a main topic in catalytic study and surface science. These studies have dealt with a variety of species of transition metals such as clusters, alloys, and inorganic salts, and especially those pertinent to the second- and third-row transition metals. A primary motivation for such studies is that these species play an important role in the catalytic and chemisorption processes.[1−13] With these efforts, not only is the determination of the activity for certain chemical reactions available, but also the mechanism of heterogeneous catalysis concerning active sites of transition metals can be investigated. In recent years, synthesis and characterization of organic metal complexes containing carbonyl ligands have received considerable attention.[14−25] It has been shown that these catalysts exhibit enhanced selectivity and compounds that differ in structure and properties. Thus homogeneous catalysts are also becoming more prospective.

Transition metals of the IVB through VIIIB groups have similar features of coordination propensity for the CO ligand. The standard description of bonding in metal carbonyls is one of donation from the highest occupied σ orbital of CO to the metal atom, followed by a π back-donation from the 4d (5d for heavy analogues) orbital of the metal atom to the $2\pi^*$ orbital of CO. Thus chemisorption and desorption of CO on metal surfaces can have significant effect on processes such as hydrogenation, hydrolysis, catalytic oxidation, carbonylation, and decarbonylation, and so on. For this reason, potential surfaces, dissociation energies, IR frequencies, and other properties of the transition metals interacting with CO have been studied extensively. The multiphoton decomposition process (MDP) of metal−CO complexes have been studied using LIF and the molecular beam method, respectively,[26,27] which indicate that the MDP process follows either sequential or concerted mechanism. Some of the fragments were found to be very stable in the process of laser decomposition or pyrolysis.[28−30] From this standpoint, many reports are concerned with the chemisorption and desorption of CO on metal surfaces to evaluate the IR frequencies, activation energy, and other useful properties.[31−34] Hydrogenation of CO on transition metal catalysts has also been extensively studied using experimental techniques such as XRD, LEED, TEM, etc.[35−38] Theoretically, the $Tc(CO)_6^+$, $Re(CO)_6^+$, and $HRe(CO)_5$ complexes were studied to determine the bonding dissociation energies (BDEs) and vibrational properties.[39,40] Ab initio methods such as DFT, RHF, and MP2 have been employed to investigate the BDEs for other $M(CO)_x$ species, where $x = 4-6$.[41−45] Several theoretical studies have been carried out to predict the electronic structure of the platinum metals and CO bonding.[46−49] The potential curves and electronic properties of heavier transition metals M + CO have been computed by our group,[50−57] where M includes most of the second- and the third-row transition metals from IVB through VIIIB groups except Tc, and Re.

The interaction of single transition metal atom with a molecule like CO can provide significant insight into the nature of CO chemisorption on metal surfaces. For example, the atop

* To whom correspondence should be addressed. E-mail: kbalu@asu.edu.

10.1021/jp984449e CCC: $18.00
Published on Web 04/15/1999

mode of chemisorption can be adequately modeled using the M + CO interaction. This has been exemplified well in the past, as seen from the work on Pt−CO.[57] Our computed CO stretching vibrational frequency of 2098 cm^{-1} for Pt−CO was found to be in remarkable agreement with the experimental CO stretching frequency of 2000−2100 cm^{-1} for the chemisorbed CO on Pt surface in the atop mode of chemisorption. Consequently, systematic studies of transition metal + CO for the various transition metal atoms could provide not only valuable insight into bonding but also on the nature of atop-chemisorption on metal surfaces.

Computational studies of the potential energy curves and the spectroscopic properties of the excited electronic states of M−CO could be valuable in gas-phase experimental studies on such species. Such studies are becoming increasingly feasible with the advent of supersonic jet expansion techniques.

As can be seen from the above survey, while a great deal of interest exists on the studies of interaction of CO with transition metals, the potential energy surfaces and the electronic properties for TcCO and ReCO complexes, to our knowledge, have not been computed using accurate techniques. Second, a systematic comparison of the electronic states and spectroscopic properties for M + CO (M = Zr−Pd, and Hf−Pt) species shed light on the periodic trends in the electronic properties of the M−CO species, which could model the atop mode of chemisorption.

The present study employs large-scale complete active space multiconfiguration self-consistent field (CASMCSCF) followed by multireference singles + doubles configuration interaction (MRSDCI) computations for TcCO and ReCO systems. We consider spin−orbit effects for ReCO through a relativistic configuration interaction (RCI) method. We also employ the RCI technique to include spin−orbit effects for TaCO, which was not considered in a previous report.[52] Finally, we summarize and compare the electronic properties of M + CO systems (M = Zr−Pd, and Hf−Pt) through our studies.

II. Method of Calculation

We employed relativistic effective core potentials (RECPs) taken from ref 58, which retained the outer $4s^24p^64d^65s^1$ shells for Tc and the outer $4s^24p^64d^55s^2$ shells for Re in the valence space, respectively. The 4-electron RECPs for the carbon atom and 6-electron RECPs for the oxygen atom were taken from ref 59, which retained the outer $2s^22p^2$ and $2s^22p^4$ shells in the valence space, respectively. The optimized valence (5s5p4d) Gaussian basis sets for the Tc and Re atoms were taken from ref 58. To test the effect of 4f-type functions, both CASSCF and MRSDCI computations were carried out by augmenting the Re basis set with one set of 10-component 4f functions. The 4f exponent was optimized for the $^4\Sigma^-$ ground state of ReCO. The final optimized 4f exponent for Re was found to be 0.4196. The 4s4p optimized Gaussian basis sets for the carbon and oxygen atoms from ref 59 were contracted to 3s3p. The carbon and oxygen basis sets were supplemented with one set of 3d functions taken from ref 60, with $\alpha_d = 0.75$ for carbon and $\alpha_d = 0.85$ for oxygen, respectively. We have found it unnecessary to include 4f-type functions.[54] In fact, the choices of 5s5p4d for the metal atoms and (3s3p1d) for the oxygen and carbon atoms, respectively, were gauged to be accurate in many of our previous reports.[50−57] This is due to the fact that the $4s^2$-$4p^6$ ($5s^25p^6$ for heavier analogues) subshells of the transition metals from IVB through VIIIB groups (except for Pd and Pt) do not participate in bonding and thus the basis functions which correspond to these shells can be contracted. A set of 3d polarization functions was included for carbon and oxygen atoms for the sake of the polarization of CO induced by the metal atom.

TABLE 1: Reference Configurations for the RCI Calculations of Re−CO near Minimum[a]

configurations					λ-s	$\omega-\omega$ states			
1σ	2σ	3σ	1π	1δ	state	1/2	3/2	5/2	7/2
2	2	1	2	2	$^6\Sigma^+$	30	29	25	24 ($^4\Delta$)
2	1	1	3	2	$^6\Pi$	32	38	30	26
2	1	0	4	2	$^4\Sigma^-$	5	5		
2	1	1	4	1	$^4\Delta$	2	6	6	2
2	2	0	3	2	$^4\Pi$	12	10	10	
total reference configurations						81	88	71	52
total determinants						11431	11779	9996	8690

[a] Re−C from 1.3 to 2.4 Å.

The TcCO and ReCO species were computed in the C_{2v} point group with the *z*-axis chosen as the C_2 axis. According to the low-lying spectral terms of the technetium and rhenium[61] atoms, we calculated the first root at the CASMCSCF level for each electronic state of all possible spin multiplicities and different bond lengths. The $(n-1)s^2(n-1)p^6$ subshells of Tc and Re, and the 2s and 2p orbitals of oxygen atom, were kept inactive in that excitations from these orbitals were not allowed, while the remaining six a_1, two b_2, two b_1, and one a_2 representations in the C_{2v} group were included in the active space. In this case, nine electrons were distributed in all possible ways among the orbitals in the active space. This choice of active and inactive spaces, namely, $n_a = 6, 2, 2, 1$ (a_1, b_2, b_1, a_2) and $n_i = 4, 2, 2, 0$, yields the correct assignments at the dissociation limit for both TcCO and ReCO.

The MRSDCI calculations were carried out for the low-lying states, in which single and double excitations from a chosen set of reference configurations were allowed. The reference configurations for the MRSDCI computations were chosen from the preceding CASMCSCF calculations with coefficients ≥ 0.05. The trial wave functions were also based on the calculational results at the CASMCSCF level. The CASMCSCF computations included up to 19 264 configuration spin functions (CSFs), while the MRSDCI computations included up to 1.0 million CSFs.

The relativistic configuration interaction (RCI) calculations that included low-lying electronic configurations of different spatial and spin symmetries in the presence of the spin−orbit operator were carried out to compute the spin−orbit contributions to the electronic states. The configurations corresponding to the low-lying states were used as reference configurations along with singly and doubly excited configurations originating from the reference configurations. Tables 1 and 2 show a list of reference configurations and their corresponding λ's as well as $\omega-\omega$ states of ReCO. We included excitations from the outermost 9 electrons in the RCI. Single and double excitations from these reference configurations generated up to 14 262 determinants. Due to the fact that the leading configurations of some nonrelativistic electronic states changed at the dissociation limit, we prepared two types of reference configurations for bond lengths varying from 1.3 to 2.4 Å, and from 2.4 to 8.0 Å. Consider the $\Omega = {}^1/_2$ state in Tables 1 and 2 as an example; for the ReCO complex near the equilibrium structure, this state contains 30 reference configurations from $1\sigma^22\sigma^23\sigma^11\pi^21\delta^2$ ($^6\Sigma^+$), 32 reference configurations from $1\sigma^22\sigma^13\sigma^11\pi^31\delta^2$ ($^6\Pi$), 5 reference configurations from $1\sigma^22\sigma^11\pi^41\delta^2$ ($^4\Sigma^-$), 2 reference configurations from $1\sigma^22\sigma^13\sigma^11\pi^41\delta^1$ ($^4\Delta$), and 12 reference configurations from $1\sigma^22\sigma^21\pi^31\delta^2$ ($^4\Pi$), with a total of 11 431 determinants. At the dissociation limit, while the reference

TABLE 2: Reference Configurations for the RCI Calculations of Re−CO at the Dissociation Limit[a]

configurations						$\omega-\omega$ states			
1σ	2σ	3σ	1π	1δ	λ-s state	1/2	3/2	5/2	7/2
2	2	1	2	2	$^6\Sigma^+$, $^4\Delta$, $^4\Sigma^-$	30	29	25	24 ($^4\Delta$)
2	1	1	3	2	$^6\Pi$	32	38	30	26
2	2	1	3	1	$^4\Pi + {}^4\Phi$	16	16	16	12 ($^4\Phi$)
2	2	1	1	3	$^4\Pi + {}^4\Phi$	16	16	16	12 ($^4\Phi$)
total reference configurations						94	99	87	74
total determinants						14198	14262	13365	11549

[a] Re−C from 2.4 to 8.0 Å.

TABLE 3: Reference Configurations for the RCI Calculations of Ta−CO near Minimum

configurations						λ-s	$\omega-\omega$ states[a]		
1σ	2σ	3σ	1π	2π	1δ	state	1/2	3/2	5/2
2	2	1	4	2	2	$^6\Sigma^+$	30	29	25
2	2	2	4	2	1	$^4\Delta$	10	10	10
2	2	2	4	3	0	$^2\Pi$	2	2	
2	2	1	4	3	1	$^4\Pi$	16	16	16
total reference configurations							58	57	51
total determinants							13697	13452	12237

[a] The $\Omega = {}^7/_2$ state need not be calculated as it arises only from the $^4\Delta$ state.

configurations from the $^4\Delta$ and $^4\Sigma^-$ nonrelativistic electronic states merge with those from the $^6\Sigma^+$state, the number of reference configurations from the $^4\Pi + {}^4\Phi$ states also increases to 32, thus leading to a total of 14 198 determinants. As expected, each relativistic potential curve connected smoothly at 2.4 Å. This choice also led to correct energy separations at the dissociation limit. Table 3 shows a list of reference configurations included in the RCI for the various Ω states of TaCO. The trial MRSDCI wave functions were based on ref 52. For the TaCO complex, 13 electrons were allowed for single and double excitations from these reference configurations that generated up to 13 697 determinants. All CASMCSCF/MRSDCI calculations were made using the modified version of ALCHEMY II[62] to include RECPs.[63] The spin−orbit integrals derived from RECPs using Pitzer's Argos[64] codes were transformed in the MRSDCI natural orbitals obtained in the absence of spin−orbit coupling. The RCI computations were based on the general RCI method for polyatomics.[65]

III. Results and Discussion

A. Atomic Energy Separations of Tc and Re. Table 4 compares our computed energy separations of TcCO and ReCO at the dissociation limits of the various molecular states together with the *J*-averaged experimental atomic splitting values from ref 61. As can be seen from Table 4, our computed results are in good agreement with the experimental values, indicating a very good reproduction of experimental results by the computed potential curves at the asymptotic region. The gross Mulliken population of the a^6S ground state of the Tc atom is computed as $4d^{5.015}5s^{1.847}$, which is in excellent agreement with the anticipated configuration of $4d^55s^2$. We have obtained an averaged dissociation limit for the $^4\Pi$, $^4\Delta$, and $^4\Phi$ states of TcCO since the ^4P, ^4F, and ^4G atomic spectral terms of the technetium atom are quite close to each other,[61] and it is thus difficult to make a definitive determination of the atomic states from the molecular computations.

The gross Mulliken population of the a^6S ground state of Re atom is computed as $5d^{4.972}6s^{1.916}$ compared to the anticipated configuration of $5d^56s^2$. Unlike the doublet states of TcCO, which are too high to be considered, the $^2\Pi$ and $^2\Delta$ states of ReCO arise from the a^2F atomic spectral term. The r_e and ω_e values for CO obtained from the MRSDCI at the M + CO dissociation limit are 1.121 Å and 2227 cm^{-1} compared to experimental values of 1.128 Å and 2170 cm^{-1} in ref 66.

B. Potential Energy Curves of Tc−CO and Re−CO. Figure 1 shows the CASMCSCF potential energy curves of the low-lying electronic states of TcCO. It is evident from our results that the $^4\Sigma^-$ state is the ground state for the TcCO complex, while a repulsive state, namely $^6\Sigma^+$, is found to be the lowest in energy at the dissociation limit region. The $^6\Sigma^+$ state arises from the Tc(a^6S) + CO($^1\Sigma^+$) dissociation limit, while the lowest excited state at the equilibrium geometry region, namely $^6\Pi$, arises from the Tc(a^6D) + CO($^1\Sigma^+$) dissociation limit. In this case, the potential energy curve of the $^6\Sigma^+$ state intersects with the $^4\Sigma^-$ and $^6\Pi$ curves near R(Tc−C) = 2.75 Å as seen from Figure 1. The intersection between the $^4\Pi$ and $^4\Phi$ states is very interesting and suggests a rearrangement of electrons in the TcCO complex, as the CO ligand dissociates from Tc.

Figure 2 shows the CASMCSCF potential energy curves of the low-lying electronic states for the ReCO system. These curves are substantially similar to those of TcCO in Figure 1 in that the $^4\Sigma^-$, $^6\Pi$, and $^4\Pi$ states are the lowest-lying molecular electronic states, while the $^6\Sigma^+$ state repulsive state is the lowest

TABLE 4: Atomic Energy Separations of Tc and Re Obtained from Asymptotic Molecular Energy Separations at the Dissociation Limit[a,b]

molecular state	dissociation limit of M + CO	CASMCSCF (cm^{-1})	MRSDCI (cm^{-1})	expt (cm^{-1})[c]
	Tc + CO			
$^6\Sigma^+$	($4d^55s^2$) a $^6S + {}^1\Sigma^+$	0	0	0
$^6\Pi$	($4d^65s$) a $^6D + {}^1\Sigma^+$	4212	5866	3277
$^4\Sigma^-$, $^4\Pi$, $^4\Delta$, $^4\Phi$	($4d^65s$) [$^4D + {}^4P + {}^4F + {}^4G$] + $^1\Sigma^+$	14908[d]	11865[d]	11030−16179[e]
	Re + CO			
$^6\Sigma^+$	($5d^56s^2$) a $^6S + {}^1\Sigma^+$	0	0	0
$^6\Pi$	($5d^66s$) a $^6D + {}^1\Sigma^+$	13436	13037	14190
$^4\Sigma^-$, $^4\Pi$, $^4\Delta$, $^4\Phi$	($5d^56s^2$) [$^4P + {}^4G$] + $^1\Sigma^+$	20595[d]	15381[d]	12928−15735[f]
2Δ, $^2\Pi$	($4d^55s^2$) a $^2F + {}^1\Sigma^+$	29998	28387	22911

[a] The distance between Re−C is 8.00 Å. [b] The r_e and ω_e values for CO obtained from the MRSDCI are 1.121 Å and 2227 cm^{-1} compared to experimental values of 1.128 Å and 2170 cm^{-1} in ref 66. [c] The experimental data are *J*-averaged values from ref 61. [d] Averaged values at both CASMCSCF and MRSDCI levels. [e] The averaged energy separation of [$^4P + {}^4D + {}^4F + {}^4G$] state with respect to the $^6\Sigma^+$ state is between 11 030 and 16 179 cm^{-1}. [f] The averaged energy separation of [$^4P + {}^4G$] state with respect to the $^6\Sigma^+$ state is between 12 928 and 15 735 cm^{-1}.

TABLE 5: Spectroscopic Properties and Energy Separations of Electronic States of TcCO[a]

	CASMCSCF					MRSDCI				
state	Tc−C (Å)	C−O (Å)	T_e (cm^{-1})	ω_e (cm^{-1})	D_e (eV)	Tc−C (Å)	C−O (Å)	T_e (cm^{-1})	ω_e (cm^{-1})	D_e (eV)
$^6\Sigma^+$					0					0
$^4\Sigma^-$	1.846	1.160	0	2208	−0.115	1.845	1.160	0 (0)	2206	0.002
$^6\Pi$	2.112	1.137	4269	2153	−0.644	2.124	1.135	4668 (5785)	2161	−0.577
$^4\Pi$	1.962	1.139	7848	2170	−1.088	1.952	1.137	6495 (6064)	2170	−0.778
$^4\Delta$	2.157	1.146	12084	2196	−1.613	2.139	1.147	11619 (12876)	2198	−1.438

[a] The ω_e stands for the vibrational frequencies between C and O atoms. The values in parentheses are Davidson corrected energies.

TABLE 6: Spectroscopic Properties and Energy Separations of Electronic States of ReCO without Spin−Orbit Effects[a]

	CASMCSCF					MRSDCI				
state	Re−C (Å)	C−O (Å)	T_e (cm^{-1})	ω_e (cm^{-1})	D_e (eV)	Re−C (Å)	C−O (Å)	T_e (cm^{-1})	ω_e (cm^{-1})	D_e (eV)
$^6\Sigma^+$					0					0
$^4\Sigma^-$	1.836	1.167	0	2219	−0.506	1.831	1.165	0 (0)	2212	0.012
$^4\Pi$	1.936	1.142	6084	2189	−1.259	1.910	1.143	3248 (2768)	2189	−0.391
$^6\Pi$	2.036	1.145	3799	2187	−0.977	2.036	1.143	4973 (5871)	2183	−0.605
$^2\Delta$	1.830	1.158	7701	2206	−1.461	1.821	1.157	5691 (5076)	2205	−0.694
$^2\Pi$	1.891	1.145	14825	2196	−2.344	1.888	1.144	13100 (11465)	2191	−1.613
$^4\Delta$	1.937	1.147	19026	2201	−2.864	1.944	1.146	19270 (19191)	2187	−2.377

[a] The ω_e stands for the vibrational frequencies between C and O atoms. The values in parentheses are the Davidson corrected energies.

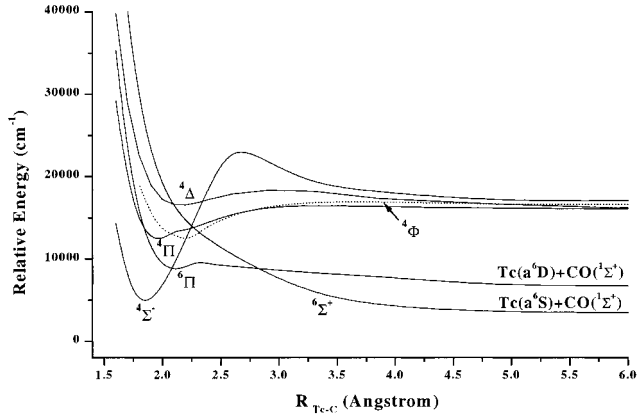

Figure 1. Potential energy curves for Tc−CO.

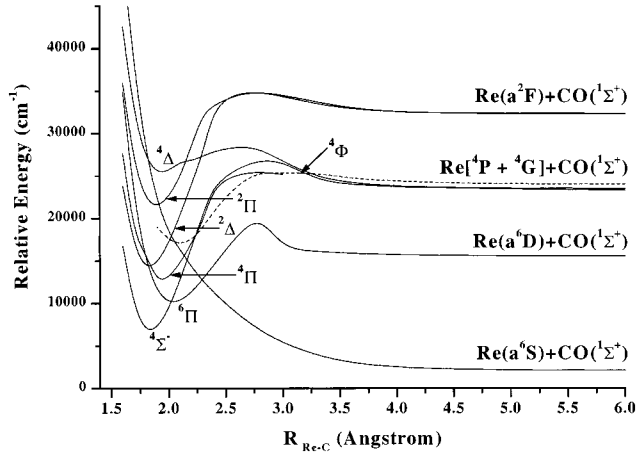

Figure 2. Potential energy curves for Re−CO.

state at the dissociation limit. Likewise the $^4\Pi$ state intersects with the $^4\Phi$ state.

Tables 5 and 6 show the actual equilibrium geometries, spectroscopic properties, and relative energy separations of the bound electronic states of TcCO and ReCO at both CASMCSCF and MRSDCI levels. The T_e column lists the minimum-minimum relative energy separations for the bound states. The dissociation energy is defined relative to the Tc(a^{6}S) + CO($^1\Sigma^+$) dissociation limit. As can be seen from Table 5, the D_e of the $^4\Sigma^-$ ground state of TcCO is computed as −0.115 and 0.002 eV at the CASMCSCF and MRSDCI levels, respectively. As expected, higher level of CI calculation usually increases the magnitude of D_e as more configurations are included in the MRSDCI. The Tc−C and C−O equilibrium bond lengths for of this state are found to be 1.933 and 1.157 Å at the CASMCSCF level, and 1.927 and 1.158 Å at the MRSDCI level, respectively. Thus, more accurate MRSDCI calculation shrinks the Tc−C bond by about 0.3%. The first excited bound state of TcCO is found to be the $^6\Pi$ state. The small difference in the energy separations between the results generated from the MRSDCI and quadruple cluster correction indicates that the reference configurations at the MRSDCI level constitute a nearly complete set. The equilibrium R_e(Tc−C) is computed as 2.112 and 2.124 Å, while R_e(C−O) = 1.137 and 1.135 Å at the CASMCSCF and the MRSDCI levels, respectively, suggest an almost unchanged carbon monoxide coordination bond length.

As seen from Table 6, analogous to TcCO, the CASMCSCF computation for ReCO yielded a negative D_e result of −0.506 eV for the $^4\Sigma^-$ ground state relative to Re(a^{6}S) + CO($^1\Sigma^+$) dissociation limit. At the MRSDCI level, this state is only 0.012 eV more stable than the same dissociation limit. The Re−C and C−O equilibrium bond lengths of the $^4\Sigma^-$ ground state are computed as 1.836 and 1.167 Å at the CASMCSCF level, and 1.831 and 1.165 Å at the MRSDCI level, respectively. The T_e's of the lowest two stable excited states, namely $^4\Pi$ and $^6\Pi$, are computed as 6084 and 3799 cm^{-1} at the CASMCSCF level, respectively. At the MRSDCI level, however, there is energy reversal in that the computed MRSDCI energy separations are 3248 and 4973 cm^{-1}, respectively. This clearly suggests the importance of higher order electron correlation effects on energy separations.

The effect of 4f type polarization functions was tested on ReCO at both CASSCF and MRSDCI levels of theory. As indicated before, the exponent for the 10-component 4f-type functions was optimized at the equilibrium geometry of the ground state of ReCO. Analogous studies including 4f-type functions were carried out earlier on IrCO[54] and the effect was found to be small. In the current study, the MRSDCI Re−C and C−O bond lengths were computed including 4f functions in the basis set as 1.82 and 1.162 Å, respectively, compared to 1.831 and 1.165 Å, respectively, obtained without the inclusion of 4f-type functions in the basis set. Thus the 4f functions shrink

TABLE 7: Atomic Energy Separations of Re−CO at the Dissociation Limit Including Spin−Orbit Effects[a]

$\omega-\omega$ states	Re + CO	ΔE(theory) (cm^{-1})	ΔE(expt) (cm^{-1})
1/2, 3/2, 5/2	$a^6S_{5/2} + {}^1\Sigma_0^+$	0	0
1/2, 3/2, 5/2, 7/2, 9/2	$a^6D_{9/2} + {}^1\Sigma_0^+$	12109	11755
1/2, 3/2, 5/2	$a^4G_{5/2} + {}^1\Sigma_0^+$	13961	14021

[a] The distance Re−C is 8.00 Å.

the Re−C bond distance by 0.01 Å, while the C−O distance is virtually unaffected. The dissociation energy obtained with 4f functions in the basis set is 0.036 eV compared to a value of 0.012 eV obtained without the 4f functions.

The general trend obtained here for the effect of 4f functions is consistent with our previous study on IrCO.[54] It was found that the Ir−C bond length decreased by 0.023 Å at the MRSDCI level due to 4f-type functions. For the excited states the change in the bond length due to 4f functions was even smaller (0.01 Å). The dissociation energy increased by 0.05 eV due to 4f type functions.

The Mulliken populations are influenced by 4f-type functions by increasing the population of the metal atom. For example, the ground state of Re total Re population increases to 14.963 with 4f-type functions compared to 14.75 without 4f functions. The oxygen population does not change at all but the C population becomes 3.495 with 4f functions on Re compared to 3.731 without 4f functions. This suggests that the 4f-type polarization functions increase the charge transfer from C to Re by 0.2. The individual Re populations are 3.056, 6.091, and 5.755 for Re(s), Re(p), and Re(d), respectively, compared to the corresponding values of 2.957, 6.070, and 5.726, respectively, obtained without 4f functions. Thus the populations in Table 10 should be adjusted by approximately this factor for the electronic states for the effect of 4f-type polarization functions on the metal atom.

There have been earlier studies on the $Tc(CO)_6^+$ and $Re(CO)_6^+$ complexes[39,40] that can be compared with our work. Compared to the calculated results in ref 39 and 40, for R(Re−C) = 2.058 Å and R(Tc−C) = 2.028 Å for $Tc(CO)_6^+$ and $Re(CO)_6^+$, respectively, and R(Re−C) = 1.987 Å for $HRe(CO)_5$, it is clear that distance between metal and carbon has to be elongated to form the octahedral complexes initiated from a linear M−CO complex, if the sequential mechanism is tenable.[26,27] Generally, the C−O equilibrium bond length for TcCO and ReCO at both CASMCSCF (1.135 Å) and MRSDCI (1.167 Å) levels remains almost unchanged, consistent with previous reports.[50−56] Our computed vibrational frequencies of C−O for TcCO and ReCO are around 2170−2212 cm^{-1}, compared to the experimental value of 2170 cm^{-1}. As seen from our results, there are allowed spectroscopic transitions that are yet to be observed. Consider the $X^4\Sigma^- - {}^6\Pi$ system of TcCO as an example; this should be an allowed transition, which is estimated to occur at 10 519 cm^{-1} based on our MRSDCI computations.

C. Spin−Orbit Effects for Re−CO. Table 7 shows the atomic energy separations of Re−CO at the dissociation limits including spin−orbit effects. Figure 3 shows the potential energy curves of the low-lying Ω state of Re−CO. These curves are obtained by applying the spin−orbit corrections derived from the RCI on the MRSDCI energies that do not include spin−orbit correction. It is evident from Table 7 and Figure 3 that all of the relativistic states have been assigned appropriately and reproduce the corresponding asymptotic dissociation limits correctly and compare well with the experimental results. The $^1/_2$, $^3/_2$, and $^5/_2$ Ω states arise from the lowest $a^6S_{5/2} + {}^1\Sigma_0^+$ dissociation limit, while the 1/2(II), 7/2 Ω states arise from the $a^6D_{9/2} + {}^1\Sigma_0^+$ dissociation limit. The energy separations between $a^6D_{9/2} + {}^1\Sigma_0^+$ and $a^6S_{5/2} + {}^1\Sigma_0^+$ asymptotes, and between $a^4G_{5/2} + {}^1\Sigma_0^+$ and $a^6S_{5/2} + {}^1\Sigma_0^+$ asymptotes are computed as 12 109 and 13 961 cm^{-1} compared to the experimental values of 11 755 and 14 021 cm^{-1} in ref 61, respectively, suggesting an excellent agreement with the experimental data.

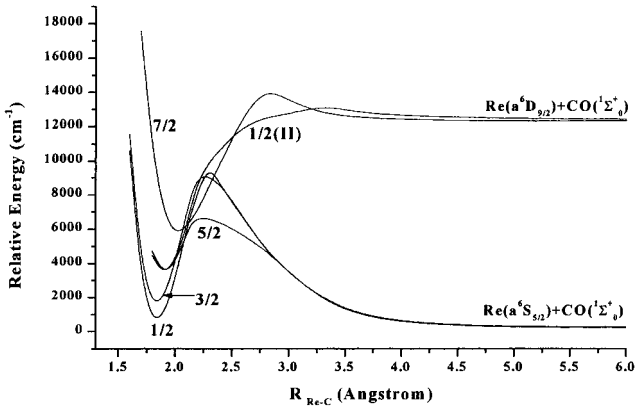

Figure 3. Potential energy curves for Re−CO including spin−orbit effects.

Table 8 shows the spectroscopic constants of the low-lying states of Re−CO including spin−orbit effects. This table compares the corrected values at the RCI level (SO) with the MRSDCI results in the absence of spin−orbit coupling (NO SO). As can be seen from Table 8 and Figure 3, the $^4\Sigma^-$ state splits into two relativistic states, namely, $\Omega = {}^1/_2$ and $^3/_2$. The $^1/_2$ state is found to be the ground state when spin−orbit coupling is included. The $^1/_2$ ground state is predominantly composed of the $^4\Sigma^-$ nonrelativistic state. The lowest excited state, viz., $^3/_2$, is predominantly composed of the $^4\Sigma^-$ state together with 5% of a $^4\Pi$ state, thus suggesting a conceivably important mixture of different nonrelativistic states. While the spin−orbit coupling has little effect on the equilibrium bond lengths and the C−O stretching frequency which is affected at most 0.5%, it splits the $^1/_2$ and $^3/_2$ states with an energy separation of 981 cm^{-1}. Moreover, the energy difference between two nonrelativistic states, e.g., $^4\Sigma^-$ and $^4\Pi$, is reduced by 1058 cm^{-1}. As to other relativistic states such as 5/2, 1/2(II), and 7/2, the spin−orbit corrections lower the T_e values at the MRSDCI level by 1763, 1717, and 1668 cm^{-1}, respectively. Thus we conclude that spin−orbit coupling on energy separations is very important.

D. Chemical Bonding of the Low-Lying States of Tc−CO and Re−CO. Table 9 shows the leading configurations of the low-lying electronic states of Tc−CO and Re−CO in the MRSDCI wave functions. Generally, the low-lying states of Tc−

TABLE 8: Spectroscopic Constants of the Low-Lying States of Re−CO Including Spin−Orbit Effects

		Re−C, Å		C−O, Å		T_e, cm^{-1}		ω_e, cm^{-1}	
$\omega-\omega$ state	main composition	SO	NO SO	SO	NO SO	SO	NO SO	SO	NO SO
1/2	>94% $^4\Sigma^-$	1.838	1.831	1.164	1.165	−1686	0	2209	2212
3/2	94% $^4\Sigma^-$, 5% $^4\Pi$	1.838	1.831	1.164	1.165	−705	0	2207	2212
5/2	92% $^4\Pi$	1.916	1.910	1.141	1.143	1485	3248	2187	2189
1/2 (II)	90% $^4\Pi$, 4% $^4\Delta$	1.907	1.910	1.141	1.143	1531	3248	2188	2189
7/2	94% $^6\Pi$	2.025	2.036	1.139	1.143	3305	4973	2207	2183

TABLE 9: Leading Configurations of the Low-Lying Electronic States of Tc−CO and Re−CO in the MRSDCI Wave Function

	weights (%)		configurations					
state	TcCO	ReCO	1σ	2σ	3σ	1π	2π	1δ
$^4\Sigma^-$	93	86	2	1		4		2
		4	2	1		2	2	2
$^6\Sigma^+$	95	93	2	2	1	2		2
$^4\Pi$	86	80	2	2		3		2
		4	2	1	1	3		2
$^6\Pi$	96	86	2	1	1	3		2
		5	2	1	1	2	1	2
$^2\Delta$		79	2	2		4		1
		7	2			4		3
$^2\Pi$		56	2	2		3		2
		16	2	1		3		3
$^4\Delta$	93	79	2	1	1	4		1
		8	2	1	1	2		3

CO are predominantly composed of a single configuration, while the low-lying states of Re−CO tend to be more complicated. Consider the $^4\Sigma^-$ ground state as an example; for Tc−CO, it is predominantly composed of $1\sigma^2 2\sigma^1 1\pi^4 1\delta^2$ with a weight of 93%, while for Re−CO, the $1\sigma^2 2\sigma^1 1\pi^2 2\pi^2 1\delta^2$ configuration makes 4% of contribution. The $^4\Pi$ low-lying state is formed by exciting an electron from the 1π to the 2σ orbitals of the $^4\Sigma^-$ ground state to form a lone pair of electrons. The $^6\Pi$ low-lying state is formed by exciting an electron from 1π to 3σ of the $^4\Sigma^-$ ground state, or by breaking up an electron from the 2σ lone pair of the $^4\Pi$ state.

Since we have kept 16 of a total 25 electrons inactive, which correspond to the $(n-1)$s and $(n-1)$p orbitals of the transition metals, and the 2s and 2p orbitals of oxygen, respectively, the remaining 9 electrons are distributed among those molecular orbitals dominated by $(n-1)$d and ns of transition metals, and 2s and 2p orbitals of carbon atom. Based on the MRSDCI wave functions of TcCO, the 1σ, 2σ, 3σ, and 1π orbitals are found to be strongly bonding. For the $^4\Sigma^-$ ground state these orbitals are composed of

$$\psi[1\sigma] = -\mathrm{C(2s)} - \mathrm{C(2p_x)} - \mathrm{Tc(5s)}$$

$$\psi[2\sigma] = -\mathrm{Tc(5)} - \mathrm{Tc(4d\sigma)}$$

$$\psi[3\sigma] = \mathrm{O(2s)} + \mathrm{O(2p_z)} - \mathrm{C(2s)} + \mathrm{C(2p_z)} + \mathrm{Tc(5s)}$$

$$\psi[1\pi] = \begin{cases} -\mathrm{C(2p_x)} + \mathrm{Tc(4d_x)} \\ -\mathrm{C(2p_y)} + \mathrm{Tc(4d_y)} \end{cases} \quad (1)$$

where the contribution of Tc (5s) is the largest in 1σ. The 1π molecular orbital is dominated by $\mathrm{Tc(4d_{xz})}$ and $\mathrm{Tc(4d_{yz})}$ with a contribution weight of 91%.

For the $^4\Sigma^-$ ground state of ReCO, the 1σ, 2σ, 3σ, and 1π orbitals are mainly composed of

$$\psi[1\sigma] = \mathrm{C(2s)} + \mathrm{C(2p_z)} + \mathrm{Re(6s)} - \mathrm{Re(5d_{x^2+y^2-2z^2})}$$

$$\psi[2\sigma] = -\mathrm{Re(6s)} - \mathrm{Re(5d_{x^2+y^2-2z^2})}$$

$$\psi[3\sigma] = \mathrm{C(2s)} + \mathrm{C(2p_z)} - \mathrm{Re(6s)} + \mathrm{Re(5d_{x^2+y^2-2z^2})}$$

$$\psi[1\pi] = \begin{cases} \mathrm{C(2p_x)} - \mathrm{Re(5d_{xz})} \\ \mathrm{C(2p_y)} - \mathrm{Re(5d_{yz})} \end{cases} \quad (2)$$

The 1π molecular orbital is composed mainly of $\mathrm{Re(5d_{xz})}$ and $\mathrm{Re(5d_{yz})}$.

The Mulliken population analysis in Table 10 reveals that the $^4\Sigma^-$ ground state of TcCO is composed of $\mathrm{Tc(4d^{6.336}5s^{0.344})}$, $\mathrm{C(2s^{1.309}2p^{2.336})}$, and $\mathrm{O(2s^{1.905}2p^{4.601})}$. If we compare these populations with the gross populations at the lowest dissociation limit for $\mathrm{Tc(a^6S)} + \mathrm{CO(^1\Sigma^+)}$, i.e., $\mathrm{Tc(4d^{5.015}5s^{1.947})}$, $\mathrm{C(2s^{1.754}2p^{1.836})}$, and $\mathrm{O(2s^{1.819}2p^{4.459})}$, it may be concluded that in order to form the TcCO complex from the ground spectral term of the metal atom (in a direct process), the carbon atom should transfer 0.45e from its 2s orbital, while the 2p orbital receives 0.5e. For the Tc atom, the 4d orbital should receive 1.32e in net charge and the 5s orbital loses 1.61e. The oxygen atom receives about 0.23e net charges. Consequently, the net charge increase for the CO ligand and the net charge decrease for Tc are nearly balanced. An alternative interpretation would involve the excited Tc atom. That is, suppose that the Tc atom is excited to the $\mathrm{Tc[^4P+^4D+^4F+^4G]}$ combination (excited process), then the electron distribution between the 4d and 5s orbitals will change from $(\mathrm{4d^5 5s^2})$ to $(\mathrm{4d^6 5s})$. The gross populations for this dissociation limit are computed as $\mathrm{Tc(4d^{6.201}5s^{0.801})}$, $\mathrm{C(2s^{1.805}2p^{1.924})}$, and $\mathrm{O(2s^{1.823}2p^{4.321})}$. Note that the $^4\Sigma^-$ ground state has been attributed to this combination dissociation limit. Thus, in order for an excited Tc atom and the CO ligand to form the TcCO complex, the carbon atom should transfer 0.50e from its 2s orbital while the 2p orbital receives 0.41e, the 4d orbital of Tc should receive 0.14e, and the Tc 5s orbital loses 0.46e. The net increase for the CO ligand and the net decrease for Tc are also nearly balanced. In this way, the charge transfer in the Tc atom becomes much less than the direct process described before. Furthermore, the large charge transfer may be facilitated by the crossings of the curves of the ground state and other low-lying excited states (as seen in Figures 1 and 2) analogous to the curve crossing seen in ionic species such as NaCl where crossing between covalent

TABLE 10: Mulliken Population Analysis for the Low-Lying Electronic States of TcCO and ReCO[a,b]

		gross population									
species	state	O	C	M	O(s)	O(p)	C(s)	C(p)	M(s)	M(p)	M(d)
TcCO	$^4\Sigma^-$	6.363	3.792	14.85	1.900	4.407	1.466	2.235	2.168	5.982	6.695
	$^6\Sigma^+$	6.323	3.677	15.00	1.819	4.459	1.754	1.836	3.847	6.139	5.015
	$^6\Pi$	6.473	3.905	14.62	1.923	4.505	1.475	2.340	2.598	6.350	5.674
	$^4\Pi$	6.456	3.718	14.83	1.900	4.510	1.361	2.260	2.027	6.057	6.742
	4Δ	6.312	3.840	14.85	1.912	4.344	1.557	2.203	2.543	6.311	5.994
ReCO	$^4\Sigma^-$	6.517	3.731	14.75	1.848	4.625	1.234	2.379	2.957	6.070	5.726
	$^6\Sigma^+$	6.315	3.685	15.00	1.824	4.447	1.777	1.830	3.916	6.112	4.972
	4Π	6.419	3.659	14.92	1.856	4.517	1.249	2.307	3.669	6.127	5.126
	$^6\Pi$	6.447	3.896	14.66	1.876	4.526	1.483	2.317	3.123	6.174	5.359
	2Δ	6.487	3.650	14.86	1.848	4.594	1.211	2.320	3.597	6.113	5.155
	$^2\Pi$	6.435	3.709	14.86	1.854	4.535	1.281	2.322	3.365	6.089	5.402
	4Δ	6.469	3.881	14.65	1.872	4.553	1.468	2.307	3.226	6.180	5.245

[a] The repulsive states were analyzed at the corresponding dissociation limits. [b] The $(n-1)\mathrm{s}^2(n-1)\mathrm{p}^6$ shells for transition metals are included.

TABLE 11: Spectroscopic Constants of the Low-Lying States of Ta−CO Including Spin−Orbit Effects

		Ta−C, Å		C−O, Å		T_e, cm^{-1}		ω_e, cm^{-1}	
$\omega-\omega$ state	main composition	SO	NO SO	SO	NO SO	SO	NO SO	SO	NO SO
1/2	88% $^4\Delta$, 4% $^6\Sigma^+$, 3% $^4\Pi$	2.055	2.063	1.144	1.143	−1611	0	2149	2151
1/2 (II)	94% $^6\Sigma^+$	2.076	2.079	1.145	1.145	131	691	2320	2321
3/2	93% $^6\Sigma^+$	2.077	2.079	1.145	1.145	285	691	2320	2321
5/2	94% $^6\Sigma^+$	2.077	2.079	1.145	1.145	502	691	2322	2321

TABLE 12: Electronic Properties and Constants of M + CO (M = Zr−Pd)[a]

	Zr	Nb	Mo[d]	Tc[e]	Ru	Rh	Pd[g]
atomic spectra[b]	$(4d^25s^2)$ a^3F_2	$(4d^45s)$ $a^6D_{1/2}$	$(4d^55s)$ a^7S_3	$(4d^55s^2)$ $a^6S_{5/2}$	$(4d^75s)$ a^5F_5	$(4d^85s)$ $a^4F_{9/2}$	$(4d^{10})$ a^1S_0
M + CO ground state	$^5\Delta$	$^6\Sigma^+$	$^5\Sigma^+$	$^4\Sigma^-$	$^3\Delta$	$^2\Delta$	$^1\Sigma^+$
R_e(M−C) (Å)	2.193	2.124	2.154	1.927	1.829	1.839	1.960
R_e(C−O) (Å)	1.155	1.146	1.113	1.158	1.152	1.146	1.140
ω_e(C−O) (cm^{-1})	2143	2135	2183	2210	2202	2127	2253
DE (eV)	0.414	0.968	−0.851	0.728	1.215	0.870	1.178
lowest excited state	$^3\Sigma^-$ [c]	$^4\Phi$	$^5\Phi$	$^6\Pi$	$^3\Sigma^-$ [f]	$^4\Delta$	$^3\Sigma^+$
R_e(M−C) (Å)	2.173	2.026	1.994	2.124	1.841	2.101	
R_e(C−O) (Å)	1.146	1.167	1.153	1.135	1.142	1.130	1.130
ω_e(C−O) (cm^{-1})	2133	2172	2196	2161	2187	2353	
DE (eV)	0.391	0.585	−1.26	−0.551	1.154	0.150	

[a] All the data are computed at the MRSDCI levels except for the case of palladium. [b] Spectra item for the ground state of metal atom. [c] Another candidate for the ground state of ZrCO. [d] The $^7\Sigma^+$ state was found to be the ground state at the dissociation limit. This state does not form minimum. [e] The $^6\Sigma^+$ state was found to be the ground state at the dissociation limit. This state does not form minimum. [f] Another candidate for the ground state of RuCO. [g] The $^3\Sigma^+$ state was found to be unbound with respect to ground-state fragments.

and ionic curves are found and there is a large charge transfer at the curve crossing. We shall discuss this further in section F.

For the ReCO complex, the $^4\Sigma^-$ ground state is composed of Re($5d^{5.726}6s^{0.957}$), C($2s^{1.234}2p^{2.379}$), and O($2s^{1.848}2p^{4.625}$), compared to the Mulliken populations at the Re(^{6}S) + CO($^1\Sigma^+$) dissociation limit (direct process), viz., Re($5d^{4.972}6s^{1.916}$), C($2s^{1.777}2p^{1.831}$), and O($2s^{1.824}2p^{4.447}$). Consequently, carbon transfers 0.54e charge from its 2s orbital while the 2p orbital accepts 0.55e charges. The 5d orbital of the rhenium atom receives 0.75e while the 6s orbital donates 0.96e. The net charge transfer between Re and CO is thus balanced. Alternatively, the Mulliken populations of the $^4\Sigma^-$ ground electronic state could be compared with the Re(a^4P) excited state (excited process). In contrast to Tc, the Re(a^4P) state term is composed of ($5d^56s^2$) primarily due to the relativistic mass−velocity stabilization of the 6s orbital of Re. The gross populations for the Re(a^4P) + CO($^1\Sigma^+$) dissociation limit are computed as Re($5d^{5.010}6s^{1.980}$), C($2s^{1.777}2p^{1.830}$), and O($2s^{1.824}2p^{4.447}$). Thus, the total charge transfer between rhenium and CO is about the same as in the direct process. In this case, in order for Re−CO to be formed, large charge transfer is inevitable.

E. Spin−Orbit Effects for Ta−CO. Table 11 shows the spin−orbit effects of the TaCO complex, which have not been addressed earlier. As seen from Table 11, the $^1/_2$ Ω state is found to be the ground state when spin−orbit effects are included. This relativistic state is mainly composed of 88% of $^4\Delta$, 4% of $^6\Sigma^+$, and 3% of $^4\Pi$. The $^6\Sigma^+$ nonrelativistic state splits to three states, namely $\Omega = {}^1/_2$, $^3/_2$, and $^5/_2$. The energy separation between the $^1/_2$ ground state and the $^1/_2$(II) state is computed as 1742 cm^{-1}, compared to 691 cm^{-1} in the absence of spin−orbit coupling for TaCO. The effect of spin−orbit coupling on other properties such as the bond lengths and the vibrational frequencies is small.

F. Periodic Trends of the Electronic Properties for M−CO Species. Since the potential energy surfaces and energy separations of the electronic states of entire second- and third-row transition metal atoms are available, it would be worthwhile to compare them and obtain general trends. Tables 12 and 13 enumerate the electronic properties of the second- and the third-row transition metals interacting with CO. All of the data on these species are obtained from ref 50 (Zr and Hf), ref 51 (Nb), ref 52 (Ta), ref 53 (Mo and W), ref 55 (Ru), ref 56 (Os), ref 54 (Rh and Ir), ref 57 (Pt), and ref 49 (Pd), as well as from the current article (Tc, Re, and Ta). Figures 4 and 5 compare the dissociation energies for the ground and the lowest excited bound states of M-CO species.

As seen from Tables 12 and 13, although the atomic spectral terms for Zr and Hf are the same (a^3F_2), the ground state of ZrCO is found to be $^5\Delta$ dominated by the $\sigma\pi^2\delta$ configuration, while the ground state of HfCO is $^3\Sigma^-$ dominated by the π^2 configuration. The $^6\Sigma^+$, $^4\Delta$, $^5\Sigma^+$, $^7\Sigma^+$, $^3\Delta$, and $^3\Sigma^-$ ground states for NbCO, TaCO, MoCO, WCO, RuCO, and OsCO are dominated by $\sigma\pi^2\delta^2$, $\pi^2\delta$, $\pi^2\delta^2$, $\sigma\sigma\pi^2\delta^2$, $\sigma\delta^3$, and δ^2 configurations, respectively. Note that the $^3\Sigma^-$ state can arise from either π^2 or δ^2 configurations. The $^4\Sigma^-$ ground state for TcCO/ReCO, the $^2\Delta$ ground states of RhCO/IrCO, and the $^1\Sigma^+$ ground state for both PdCO/PtCO are dominated by $\sigma\delta^2$, δ^3, and σ^2 closed-shell configurations, respectively. Most of the leading configurations have made at least 85% of contribution to the formation of the ground state. As expected, electronic states of higher spin multiplicities such as quintet, sextet, and even septet occur for NbCO, MoCO, and TcCO, and their heavier analogues, as these metal atoms exhibit more singly occupied d electrons. Meanwhile, the largest charge transfer also occurs from the MoCO/WCO through TcCO/ReCO species. This seems to explain the unusual stability of these four species in contrast to other M−CO systems.

As can be seen from many reports, the potential energy curves of the ground states of these species often intersect with the curves of other low-lying electronic states. Specifically, for most of the second- and third-row M−CO systems (with the only exception of HfCO, NbCO, and TaCO), the ground state of M−CO does not arise from the ground spectral term of the corresponding metal atom. This is true for many systems such as ReCO, OsCO, and IrCO, etc., thus making it inevitable for the existence of intersection between the ground state and some low-lying excited states. The curve crossings between the ground and excited states facilitate charge transfer. Consider TcCO as an example; the $^4\Sigma^-$ ground state arises from an averaged quartet ($4d^65s$) atomic spectral term, which is approximately 11 865

TABLE 13: Electronic Properties and Constants of M + CO (M = Hf−Pt) Including Spin−Orbit Effects[a]

	Hf	Ta	W	Re [d]	Os	Ir	Pt
atomic spectra[b]	$(5d^26s^2)\ a^3F_2$	$(5d^36s^2)\ a^4F_{3/2}$	$(5d^46s^2)\ a^5D_0$	$(5d^56s^2)\ a^6S_{5/2}$	$(5d^66s^2)\ a^5D_4$	$(5d^76s^2)\ a^4F_{9/2}$	$(5d^96s)\ a^3D$
M + CO ground state (NO SO)	$^3\Sigma^-$	$^4\Delta$	$^7\Sigma^+$	$^4\Sigma^-$	$^3\Sigma^-$	$^2\Delta$	$^1\Sigma^+$
R_e(M−C) (Å)	2.126	2.063	2.195	1.831	1.795	1.772	1.900
R_e(C−O) (Å)	1.156	1.143	1.123	1.165	1.148	1.161	1.147
ω_e(C−O) (cm^{-1})	2153	2151	2176	2212	2129	2074	2099
DE (eV)	0.922	0.929	0.276	0.012	1.357	2.13	1.862
lowest excited state (NO SO)	$^1\Delta$	$^6\Sigma^+$	$^5\Phi$	$^4\Pi$	$^3\Delta$	$^4\Delta$	$^3\Sigma^+$
R_e(M−C) (Å)	2.134	2.142	1.960	1.910	1.799	1.943	2.024[e]
R_e(C−O) (Å)	1.161	1.128	1.157	1.143	1.156	1.146	1.126[e]
ω_e(C−O) (cm^{-1})	2154	2320	2202	2189	2127	2128	1914[f]
DE (eV)	0.545	0.846	0.244	−0.391	0.605	0.94	0.612
M + CO ground state (SO)	$^3\Sigma_0^+$	$4\Delta_{1/2}$	$^7\Sigma_1^+$ [c]	$4\Sigma_{1/2}^-$	$^3\Sigma_0^+$	$2\Delta_{5/2}$	$^1\Sigma_0^+$
lowest excited state (SO)	$^3\Sigma_1^-$	$6\Sigma_{1/2}^+$	$^7\Sigma_2^+$	$^4\Sigma_{3/2}^-$	$^3\Sigma_1^-$	$2\Delta_{3/2}$	$^3\Sigma_1^+$ [g]
evaluation of the maximal spin−orbit splitting (cm^{-1})	193	1051	450	1058	2770	6852	3549[h]

[a] All the data without spin−orbit effects are computed at the MRSDCI levels. [b] Spectra item for the ground state of metal atom. [c] This state is converged to $^5D_1$ atomic state at the dissociation limit. [d] The $^6\Sigma^+$ state was found to be the ground state at the dissociation limit. This state does not form minimum. [e] At the CASMCSCF level [f] Reference 49. [g] Assumed. [h] Among triplet states.

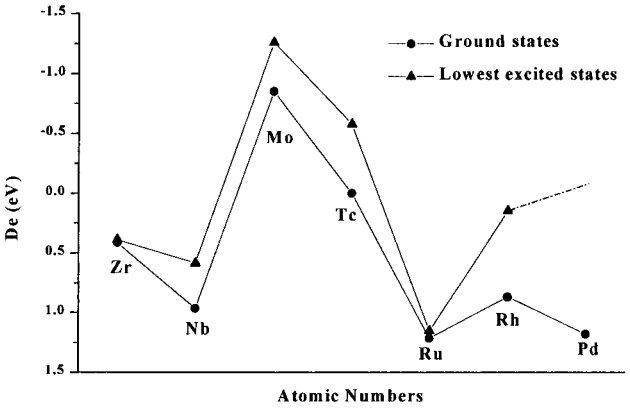

Figure 4. Dissociation energies for the ground and the lowest excited states of M−CO, M = Zr−Pd.

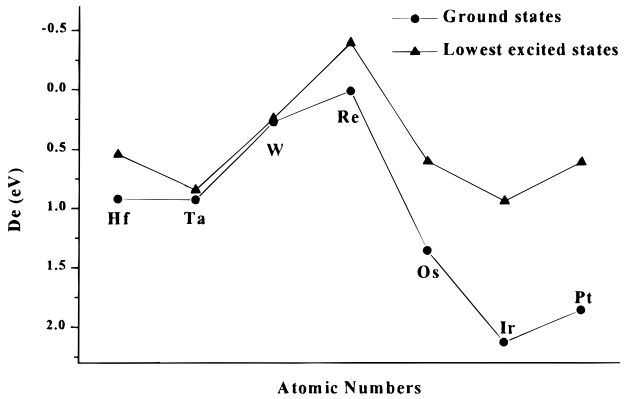

Figure 5. Dissociation energies for the ground and the lowest excited states of M−CO, M = Hf−Pt.

cm^{-1} higher than the ground atomic spectral term ^6S ($4d^55s^2$). Thus, according to the gross population analysis, in order to form the $^4\Sigma^-$ ground state, the Tc atom should donate 0.633e from its 5s orbital and receive 0.494e through its 4d orbital, relative to the ^4D atomic spectral term that generates the $^4\Sigma^-$ ground state. Alternatively, the Tc atom should altogether donate 1.679e from its 5s orbital and receive 1.524e through its 4d orbital, relative to the ^6S ground atomic spectral term. Regardless of the route, the Tc atom loses 0.15e of net charge density. Note that the electronic distributions for the ^6S and ^4D states are considerably different. From this standpoint, it is the readjustment of the electronic distribution that leads to the intersection of the ground state with other low-lying electronic states, and the intersection generates a large charge transfer. As can be seen from our gross population results, there is no evidence whether or not the *n*s and (*n* − 1)d orbitals of the metal atoms will lose and accept electronic charges, respectively, as clearly exhibited in the cases of 5σ and 2π orbitals of CO. For example, according to the net gross population analysis for the ground state of the M−CO species and the ground spectral term of the corresponding atoms, the 6s orbital of Ta accepts 0.20e while the 5d orbital loses 0.44e. In contrast, for HfCO, both the 6s and 5d orbitals of Hf lose electronic charge density. For other species such as RuCO and RhCO, the 5s orbital donates greater electronic density. Thus, in order for the M−CO system to be formed, the electronic charges on the *n*s and (*n* − 1)d orbitals will have to be rearranged so that the gross population of the metal atom is less than the pure atomic population, although in many cases, it is indeed that the *n*s orbital of the atom donates greater charge density than (*n* − 1)d. Second, the 6s orbitals (for Hf−Pt) have greater propensity to accept charges than the 5s orbitals (Zr−Pd) due to the relativistic mass−velocity stabilization of the 6s orbitals. The decreased stability of the MoCO/WCO through TcCO/ReCO species compared to other M−CO systems is attributed to the large charge transfer. As can be seen from our reports, the largest charge transfer also occurs at the MoCO/WCO through TcCO/ReCO region. Thus, these species are stabilized through considerably larger charge transfer.

Figures 4 and 5 exhibit the dissociation energies for the ground and the lowest excited bound states of the M−CO systems, where M stands for the second- and third-row transition metals Zr−Pd and Hf−Pt. As can be seen from Figures 4 and 5 together with Tables 12 and 13, three nearly degenerate electronic states exist for ZrCO, RuCO, and WCO, while for TcCO and IrCO, the energy separations between two lowest lying states are considerably higher. Consider ZrCO as an example; the energy difference between $^5\Delta$ and the competitive $^3\Sigma^-$ state is only 0.023 eV. This suggests that both states can be considered as viable candidates for the ground state. The negative dissociation energies for M−CO species occur at MoCO and TcCO. In this region, we have also found some other important features, such as unbound $^n\Sigma^+$ states ($n = 6$ for Tc/Re and 7 for Mo/W) which dissociate into the lowest dissociation limit, and crossings between $^m\Pi$ and $^m\Phi$ ($m = 4$ for Tc/Re and 5 for Mo/W). On the other hand, NbCO, RuCO, RhCO, and PdCO and their heavier analogues are unambigu-

ously more stable. For example, the dissociation energy of Ir−CO is even up to 2.13 eV. Basically, the heavier analogues form more stable complexes with CO than the lighter species, as the 6s orbital has enhanced propensity to accept electronic charge density donated by CO, due to the relativistic mass−velocity stabilization of the 6s orbital of the third-row transition metal atoms. Approximately, the curve patterns in Figures 4 and 5 are very much alike, thus suggesting a periodic trend for the interaction and dissociation of transition metals with CO.

The shortest bond length of M−C occurs at IrCO with R(Ir−C) = 1.772 Å at the MRSDCI level. On the other hand, the longest bond length of M−C is R(W−C) = 2.195 Å at the MRSDCI level. The C−O bond length does not vary much, ranging from 1.113 to 1.167 Å all through Tables 12 and 13. The ω_e of the CO bond is shifted from 1914 to 2353 cm^{-1}, thus generating a wide range of frequencies for the various M−CO systems. As seen from Table 13, the spin−orbit effects of the third-row transition metals interacting with CO exhibit the following trends: (1) for M−CO species, the spin−orbit splitting increases with respect to atomic numbers; (2) the spin−orbit effects for M−CO with half-integral Ω values are generally higher. For example, the largest splitting is exhibited by IrCO, for which spin−orbit splitting is 6852 cm^{-1}. It is evident from our investigation that large relativistic effects have made great contribution to the stabilization of OsCO, IrCO, and PtCO species. And, this can partly explain why transition metals such as Pd, Ir, and Pt are frequently used as active sites for CO adsorption.

IV. Conclusion

The potential energy surfaces of TcCO and ReCO were obtained by using the CASMCSCF followed by MRSDCI methods. The RCI technique was employed to include spin−orbit effects for the ReCO and TaCO species. The $^4\Sigma^-$ state is found to be the ground state for TcCO with R(Tc−C) = 1.933 Å and R(C−O) = 1.157 Å at the CASMCSCF level, and R(Tc−C) = 1.927 Å and R(C−O) = 1.158 Å at the MRSDCI level, respectively. The $^4\Sigma^-$ state, although very stable relative to its own quartet dissociation limit, is barely stable with respect to the lowest dissociation limit of Tc(a^6S) + CO($^1\Sigma^+$). For ReCO, the same $^4\Sigma^-$ state is found to be the ground state with equilibrium geometries of R(Re−C) = 1.836 Å and R(C−O) = 1.167 Å at the CASMCSCF level, and R(Re−C) = 1.831 Å and R(C−O) = 1.165 Å at the MRSDCI level, respectively. Analogous to TcCO, this state is only 0.012 eV lower in energy relative to the Re(a^6S) + CO($^1\Sigma^+$) dissociation limit. At the RCI level, the $^1/_2$ state is computed as the ground state, and the spin−orbit splitting is 1058 cm^{-1}. The $^6\Pi$, $^4\Pi$, and the repulsive $^6\Sigma^+$ states are found to be other low-lying states for TcCO and ReCO. The bonding nature of the low-lying electronic states for TcCO and ReCO is discussed through the CI coefficients and the Mulliken populations. An unusually large charge transfer has been found for both TcCO and ReCO. The unexpectedly decreased stability of ReCO compared to TcCO may be attributed to the large electronic charge transfer interaction mentioned above. For TaCO, the $^1/_2$ state that is dominated by the $^4\Delta$ nonrelativistic state is found to be the ground state with a spin−orbit splitting of 1051 cm^{-1}.

We have summarized the chemical bonding and the electronic properties of M−CO species to shed light on the periodic trends: (1) the third-row transition metals react more readily with CO than the lighter analogues do; (2) the spin−orbit effects for M−CO with half-integral Ω values are generally higher; (3) MoCO/WCO through TcCO/ReCO are relatively less stable, while the most stable M−CO species were found to be those formed by Os, Ir, and Pt, and their lighter analogues at the periodic table. The spin−orbit effects of OsCO, IrCO, and PtCO are dramatically larger.

Acknowledgment. This research was supported by the U.S. Department of Energy under Grant No. DEFG02-86ER13558 and the China CHPCC center.

References and Notes

(1) Pestryakov, A. N.; Davydov, A. A. *Kinet. Catal.* **1996**, *37*, 859.
(2) Lei, X. J.; Shang, M. Y.; Fehlner, T. P. *Organometallics* **1997**, *16*, 5289.
(3) Al-Shammary, A. F. Y.; Caga, I. T.; Tata, A. Y. *J. Chem. Technol. Biotechnol*. **1992**, *55*, 375.
(4) Lou, J. R.; Wong, P. C.; Mitchell, K. A. R. *Can. J. Chem*. **1988**, *66*, 3157.
(5) Imada, Y.; Shido, T.; Ichikawa, M. *Catal. Lett*. **1996**, *38*, 101.
(6) Takeishi, K.; Aika, K. *Appl. Catal., A, Gen*. **1995**, *133*, 31.
(7) Shen, J. Y.; Sayari, A.; Kaliaguine, S. *Appl. Spectrosc*. **1992**, *46*, 1288.
(8) Shimomura, H.; Lei, X. J.; Fehlner, T. P. *Organometallics* **1997**, *16*, 5302.
(9) Curtis, M. A.; Houser, E. J.; Grimes, R. N. *Inorg. Chem.* **1998**, *37*, 102.
(10) Abbott, A. P.; Malkov, A. V.; Kocovsky, P. *Organometallics* **1997**, *16*, 3690.
(11) Xu, L.; Li, Z. F.; Huang, J. S. *Inorg. Chem.* **1996**, *35*, 5097.
(12) Shapley, J. R.; Hsu, G. S.; Wilson, S. R. *Inorg. Chem*. **1996**, *35*, 923.
(13) Taniguchi, M.; Ishii, Y.; Hidai, M. *J. Chem. Soc., Chem. Commun*. **1995**, *24*, 2533.
(14) Gibson, D. H.; Mehta J. M.; Richardson, J. F. *Organometallics* **1995**, *14*, 4886.
(15) Ellis, J. E.; Frerichs, S. R.; Stein, B. K. *Organometallics* **1993**, *12*, 1048.
(16) Erker, G.; Brackemeyer, T.; Frohlich, R. *Organometallics* **1997**, *16*, 531.
(17) Howard, W. A.; Trnka, T. M.; Parkin, G. *Organometallics* **1995**, *14*, 4037.
(18) Diamond, M. G.; Green, L. H. M.; Popham, A. N. *J. Chem. Soc., Dalton Trans.* **1993**, *16*, 2535.
(19) Braunstein, P.; Cauzzi, D.; Kelly, D. *Inorg. Chem*. **1993**, *32*, 3373.
(20) Veith, M.; Mathur, S.; Huch, V. *J. Chem. Soc., Dalton Trans*. **1997**, *12*, 2101.
(21) Ellis, J. E.; Chi, K. M. *J. Am. Chem. Soc*. **1990**, *112*, 6022.
(22) Alper, H.; Crudden, C. M. *J. Org. Chem*. **1995**, *60*, 5579.
(23) Chatani, N. *J. Am. Chem. Soc*. **1993**, *115*, 11614.
(24) Cook, D. J.; Hill, A. F. *Organometallics* **1997**, *16*, 5616.
(25) Rossignoli, M.; Bernhardt, P. V.; Lwarance, G. A. *J. Chem. Soc., Dalton Trans.* **1997**, *22*, 4247.
(26) Trushin, S. A.; Sugawara, K.; Takeo, H. *Chem. Phys. Lett*. **1995**, *236*, 402.
(27) Venkataraman, B.; Hou, H. Q.; Zhang, Z. J.; Chen, S. H.; Bandukwalla, G.; Vernon, M. *J. Chem. Phys.* **1990**, *92*, 5338.
(28) Lewis, K. E.; Golden, D. M.; Smith, G. P. *J. Am. Chem. Soc*. **1984**, *106*, 3905.
(29) Ang, H. G.; Chan, K. S.; Neo, S. K. *J. Chem. Soc., Dalton Trans*. **1995**, *23*, 3753.
(30) Williams, C. C.; Ekerdt, J. G. *J. Phys. Chem.* **1993**, *97*, 6843.
(31) Morterra, C.; Orio, L.; Emanuel, C. *J. Chem. Soc., Faraday Trans*. **1990**, *86*, 3003.
(32) Yang, S.; Li, C.; Xin, Q. *Chem. Commun*. **1997**, *13*, 1247.
(33) Erickson, J. W.; Estrup, P. J. *Surf. Sci*. **1986**, *167*, 519.
(34) Escalona, P. E.; Penarroya, M. M. *Inorg. Chem*. **1994**, *33*, 1506.
(35) Lee, J. S.; Lee, K. H.; Lee, J. Y. *J. Phys. Chem*. **1992**, *96*, 362.
(36) Silver, R. G.; Hou, C. J.; Ekerdt, J. G. *J. Catal*. **1989**, *118*, 400.
(37) Tercioglu, T.; Akyurtlu, J. F. *Appl. Catal., A, Gen*. **1996**, *136*, 105.
(38) Alper, H.; Crudden, C. M. *J. Org. Chem*. **1995**, *60*, 5579.
(39) Ehlers, A. W.; Ruiz-Morales, Y.; Baerends, E. J.; Zielger, T. *Inorg. Chem*. **1997**, *36*, 5031.
(40) Jonas, V.; Thiel, W. *J. Chem. Phys*. **1996**, *105*, 3636.
(41) Ziegler, T.; Tschinke, V.; Ursenbach, C. *J. Am. Chem. Soc*. **1987**, *109*, 4825.
(42) Rosa, A.; Ricciardi, G.; Rosi, M. *J. Chem. Soc., Dalton Trans*. **1993**, *24*, 3759.
(43) Guillot, F.; Dezarnaud-Dandine, C.; Fronzoni, G. *Chem. Phys*. **1995**, *191*, 289.
(44) Jonas, V.; Thiel, W. *J. Chem. Phys*. **1995**, *102*, 8474.

(45) Li, J.; Schreckenbach, G.; Ziegler, T. *J. Am. Chem. Soc.* **1995**, *117*, 486.

(46) A. Blomberg, M. R.; Brandemark, U.; Johansson, J.; Siegbahn, P. E. M.; Wennerberg, J. *J. Chem. Phys*. **1988**, *88*, 4324.

(47) Blomberg, M. R. A.; Lebrilla, C. B.; Siegbahn, P. E. M. *Chem. Phys. Lett*. **1988**, *150*, 522.

(48) Gavezzotti, A.; Tantardini, G. F.; Simonetta, M. *Chem. Phys. Lett*. **1986**, *129*, 577.

(49) Smith, G. W.; Carter, E. A. *J. Phys. Chem*. **1991**, *95*, 2327.

(50) Tan, H.; Liao, M. Z.; Balasubramanian, K. *J. Phys. Chem*. **1998**, *102*, 1602.

(51) Tan, H.; Liao, M. Z.; Balasubramanian, K. *Chem. Phys. Lett*., submitted for publication.

(52) Majumdar, D.; Balasubramanian, K. *Chem. Phys. Lett*. **1996**, *262*, 263.

(53) Tan, H.; Liao, M. Z.; Dai, D. G.; Balasubramanian, K. *J. Phys. Chem*., in press.

(54) Dai, D.; Balasubramanian, K. *J. Chem. Phys.* **1994**, *101*, 2148.

(55) Tan, H.; Liao, M. Z.; Balasubramanian, K. *Chem. Phys. Lett*. **1998**, *284*, 1.

(56) Tan, H.; Liao, M. Z.; Balasubramanian, K. *Chem. Phys. Lett*., in press.

(57) Roszak, S.; Balasubramanian, K. *J. Phys. Chem*. **1993**, *97*, 11238.

(58) LaJohn, L. A.; Christiansen, P. A.; Ross, R. B.; Atashroo, T.; Ermler, W. C.; *J. Chem. Phys*. **1987**, *87*, 2812. Ross, R. B.; Powers, J. M.; Atashroo, T.; Ermler, W. C.; LaJohn, L. A.; Christiansen, P. A. *J. Chem. Phys*. **1990**, *93*, 6654.

(59) Pacios, L. F.; Christiansen, P. A. *J. Chem. Phys*. **1985**, *82*, 2664.

(60) Dunning, Jr. T. H.; Hay, P. J. *Methods of Electronic Structure Theory*; Schaefer, H. F., III., Ed.; Plenum Press: New York, 1977; p 1.

(61) Moore, C. E. *Tables of Atomic Energy Levels*; National Bureau of Standards: Washington, DC, 1971.

(62) The major authors of ALCHEMY II are B. Lengsfield, B. Liu, and M. Yoshimine.

(63) Balasubramanian, K. *Chem. Phys. Lett*. **1986**, *127*, 585.

(64) Pitzer, R. M.; Winter, N. W. *J. Phys. Chem*. **1988**, *92*, 3061.

(65) Balasubramanian, K. *J. Chem. Phys*. **1988**, **87**, 5731.

(66) Huber, K. P.; Herzberg, G. *Molecular Spectra and Molecular Structure IV, Constants of Diatomic Molecules*; Van Nostrand Reinhold: New York, 1979.

(67) Balasubramanian, K. *Relativistic Effects in Chemistry. Part A: Theory and Techniques*; Wiley-Interscience, New York, 1997; p 301.